# Author response to Referee #1 (RC1, essd-2026-364)

Xinhai Han, Xiaohui Li, Jingsong Yang, Hanyue Ni, Zeyi Niu, Wei Huang

All of the new verification figures below use the OCS-pass subset (the subset recommended for quantitative use in the paper, where the satellite has actually sampled the inner core), and the reference data (C-band SAR; airborne Tail Doppler Radar, TDR) are independent of IBTrACS and of the model training data. Each of your comments is reproduced in full in the grey boxes below, with our reply directly beneath it; where relevant, we indicate how the manuscript will be revised.

*This is a potentially useful dataset as surface winds in tropical cyclones are difficult to observe with the both the scarcity, quality and spatial coverage of those observations. I have my reservations about the reconstruction of the inner core wind fields and would like to see some additional validation.*

We thank you for recognising the value of the dataset and for the constructive comments on the inner-core reconstruction, particularly on vortex asymmetry and the radius of maximum wind (RMW). These are the two central difficulties in reconstructing the two-dimensional TC wind field. In response to your request for additional validation, the analyses below are all new and rest on references that are independent of the model training data, so that the radius-resolved errors, the RMW statistics and the asymmetry assessment give a concrete basis for judging which tasks the data suit.

*Verification: Two of the difficulties in reconstructing the two-dimensional wind field in tropical cyclones whether via parametric models or data fitting methods are the proper estimation of asymmetries and of the radius of maximum wind. To make this dataset more useful and provide users with confidence that these data can be used for a particular task, errors and uncertainties related to the vortex asymmetries and the location of the radius of maximum wind should be included in the write up. You can see issues related to the rmw in figure 1 and figure 2. The former shows RMW of 34 km while the aircraft based estimate is closer to 17-19 km. In figure 2 the observed by SAR rmw values are 15, 37 and 37 km, from left to right.*

*I suggest 1) providing errors and uncertainties as a function of radius either normalized by RMW or not, 2) provide statistics about the quality of the location of the radius of maximum wind, and 3) provide some estimate of the quality of the wavenumber 1 asymmetries also as a function of radius (possibly done in a motion relative framework).*

We added independent verification against C-band SAR (NOAA/STAR TC winds, the same source as the paper's SAR validation) and airborne TDR (TC-RADAR v3; Fischer et al., 2022), and address your three suggestions in turn below. For every comparison, QiFeng and the reference field *independently* relocate the eye (QiFeng on the reconstructed field; SAR by advecting the IBTrACS centre to the overpass time and re-centring under quality control), so that RMW and asymmetry are always compared about each field's own eye.

The product's core quantities, validated in Sect. 3 of the paper, are the kilometre-scale vector inner-core structure, $V_{\max}$ (OCS bias $+1.1\,\mathrm{m\,s^{-1}}$; on the full sample the absolute $V_{\max}$ bias is $\approx$79 %/75 % smaller than ERA5/CCMP) and wind direction (RMSE 28° vs. TDR). The two quantities you flag, the absolute RMW and the inner-core asymmetry amplitude, are the ones most strongly limited by the CYGNSS sampling scale, and we quantify both below. The RMW is a single scalar diagnosed from the wind field, so it is the most sampling-sensitive quantity in the product. We also take your

point that the best-track (IBTrACS) RMW is itself only an approximate reference, and that aircraft observations are considerably more reliable for inner-core structure; for that reason the assessment below leans on independent aircraft (TDR) and SAR rather than on IBTrACS. As rough context only, QiFeng's full-sample RMW bias against IBTrACS is about −7 km, against roughly +50 km for ERA5 and CCMP.

While preparing this verification we examined every time-matched SAR overpass scene by scene, and this prompted us to refine the SAR sample. C-band SAR winds are themselves noisy and are frequently degraded by eyewall heavy-rain saturation, near-coast/land contamination and incomplete coverage, so a clean, locatable eye cannot be recovered from a large fraction of the overpasses. To isolate the cases in which the SAR side does have a usable eye, we use an objective, self-validating eye detector (explicit thresholds on central data coverage, distance from the swath edge, eye–eyewall contrast and azimuthal coverage) and inspect per-scene audit sheets to check its verdicts. We also apply the wind product's own land/ice mask, which we found to be the dominant source of spurious 90–100 $\mathrm{m\,s^{-1}}$ "winds" in coastal and landfalling scenes (e.g. Ian, Kompasu, Noru). Of the ∼108 overpasses, only 45 contain a clean, well-centred eye; the rest fail because of no usable data near the centre (37), a central data gap (11), placement at the swath edge (9), or insufficient eye contrast (6). For the storm-relative (RMW / asymmetry) analyses we additionally require the *QiFeng* side to contain a clear eye passing the *same* detector, so both fields meet the same standard (this excludes, for example, Hurricane Eta on 2020-11-11, whose QiFeng field is then nearly flat with no clear eyewall). On the OCS-pass subset this leaves 22 cases with clean SAR and QiFeng eyes, of which 19 also yield a robust azimuthal-mean SAR RMW; the RMW and asymmetry analyses below therefore use these 19 cases, a stricter subset of the 47-case OCS-pass set used for the pixel-level SAR comparison in the preprint (Sect. 3.1), which aligned on the wind-minimum eye but had not yet applied this locatable-eye screen. On this inner-core-dominated subset the pixel-level errors are modestly larger than in the paper, as expected for an eyewall-dominated sample. Computed exactly as in the paper, the per-case RMSE median over these 22 cases is ≈6.0 $\mathrm{m\,s^{-1}}$ and the pooled-pixel RMSE over the 19-case structural subset is ≈6.5 $\mathrm{m\,s^{-1}}$; the paper's corresponding values are 4.88 and 5.58 $\mathrm{m\,s^{-1}}$. The increase simply reflects that the audited cases are predominantly intense storms with developed eyewalls, so the comparison now fully covers the high-error eyewall band. In the revision we will keep the 47-case pixel-level SAR validation (which is appropriate for the bulk wind-speed comparison) and will base the new RMW and asymmetry analyses on this stricter audited subset.

Your first suggestion was errors and uncertainties as a function of radius, which we show in Fig. R1.

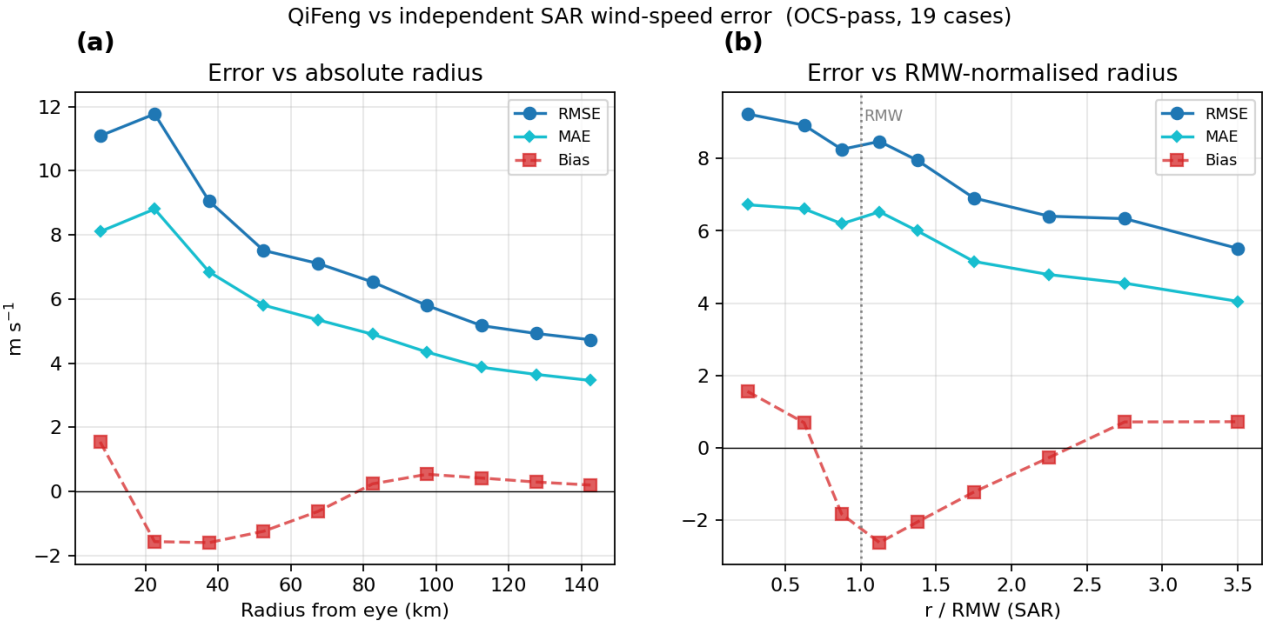

**Fig. R1.** QiFeng wind-speed error vs. radius relative to independent SAR (OCS-pass, 19 cases). (a) absolute radius; (b) radius normalised by the *per-scene SAR-derived* RMW ($r/\mathrm{RMW_{SAR}}$).

Against the independent SAR, the wind-speed RMSE is largest in the eyewall band (15–30 km, $\approx$11.8 m s$^{-1}$) and falls monotonically outward to $\approx$4.7 m s$^{-1}$ in the outer core (135–150 km), with the MAE dropping correspondingly from $\approx$8.8 to $\approx$3.5 m s$^{-1}$. Normalising the radius by the per-scene SAR-derived RMW gives the same picture: the inner-core RMSE stays near 8–9 m s$^{-1}$ (eye, $r/\mathrm{RMW}<0.5$: $\approx$9.2; eyewall, $r/\mathrm{RMW}\approx0.75$–$1.25$: $\approx$8.3–8.5) and declines gradually outward, while the bias shifts from +1.6 m s$^{-1}$ inside the eye to about −2.6 m s$^{-1}$ just outside the RMW ($r/\mathrm{RMW}\approx1.0$–$1.25$), so the peak eyewall wind is slightly underestimated. This pattern, with the largest error in the inner core and eyewall and a steady decrease outward, follows the known loss of L-band GNSS-R sensitivity at high wind speed; beyond the eyewall the agreement is good (outer-core RMSE $\approx$5 m s$^{-1}$, MAE $\approx$3.5 m s$^{-1}$) and the bias is close to zero. We will add Fig. R1 and a radius-binned error table to the technical-validation section.

Your second suggestion was statistics on the quality of the RMW location, which we summarise in Fig. R2.

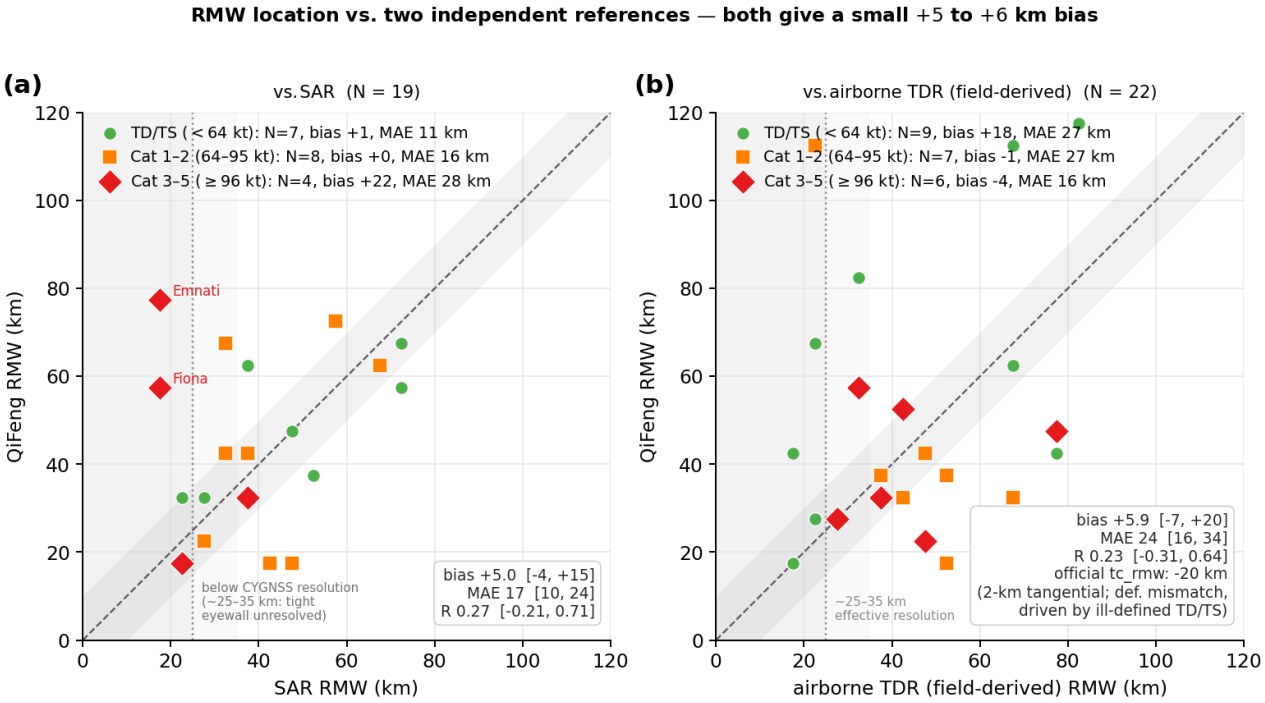


**Fig. R2.** RMW location vs. *two independent references* (OCS-pass): (a) QiFeng vs. SAR ($N$ = 19) and (b) QiFeng vs. the airborne TDR *field-derived* RMW ($N$ = 22), both computed with the *same* azimuthal-mean wind-speed definition as QiFeng so the two panels are like-for-like. Points are colour-coded by IBTrACS intensity (green: TD/TS; orange: Cat 1–2; red: Cat 3–5); the legend gives the per-class $N$, bias and MAE, and the corner box the overall bias, MAE and $R$ with 95 % bootstrap confidence intervals (CIs). Both references give the same small positive bias (+5.0 and +5.9 km). Panel (b) also annotates the bias against TC-RADAR's *official* 2 km tangential-wind `tc_rmw` (−19.6 km): this larger value reflects a different RMW convention and centring (a 2 km tangential-wind RMW in TC-RADAR's own recentred frame vs. QiFeng's surface total-wind-speed RMW), and is concentrated in weak TD/TS storms for which the operational tangential-wind RMW is itself ill defined (median $\approx$112 km); it is not a reconstruction error — where the eyewall is well defined even

the `tc_rmw` bias is small (Cat 1–2 +1.5, Cat 3–5 −2.3 km). The shaded band marks the ∼25–35 km CYGNSS effective spatial resolution (a soft floor, not a hard cut-off): in panel (a) the largest positive errors (e.g. Emnati, Fiona) occur for RMW below it, where a tight eyewall cannot be resolved; in panel (b) the residual scatter reflects both genuine reconstruction errors of either sign and the TDR reference's own RMW uncertainty, including the broad, ill-defined wind maxima of weak storms.

Against SAR, QiFeng's RMW has a bias of +5.0 km (95 % CI $[-4.5, +15]$, consistent with zero), an MAE of 16.6 km (CI $[10, 24]$) and $R = 0.27$ (CI $[-0.21, 0.71]$); 53 % of cases fall within ±10 km and 68 % within ±20 km. The small net bias, however, hides a large case-to-case scatter with errors of both signs (MAE 16.6 km, more than three times the bias) — it is small mainly because positive and negative departures cancel. Stratifying by IBTrACS intensity (Fig. R2 colours; table below) shows that the weaker TD/TS storms agree well and that the near-zero Cat 1–2 net bias arises only because offsetting errors of ±15–35 km cancel (so its 16.3 km MAE, not the near-zero bias, is the meaningful measure), while the +22.5 km mean of the four Cat 3–5 cases is driven by just two of them (Emnati +60 and Fiona +40 km, small-eye storms placed too far out); the other two (Faraji at 135 kt and Ian at 105 kt) actually agree to within 5 km. The intense-storm positive bias is therefore a tendency in some small-eye cases, not a uniform property of strong TCs.

| Intensity | $N$ | bias (km) | MAE (km) | $R$ | within ±20 km |
|---|---|---|---|---|---|
| TD/TS (<64 kt) | 7 | +0.7 | 10.7 | +0.70 | 86 % |
| Cat 1–2 (64–95 kt) | 8 | 0.0 | 16.3 | +0.40 | 63 % |
| Cat 3–5 (≥96 kt) | 4 | +22.5 | 27.5 | −0.55[†] | 50 % |
| All | 19 | +5.0 | 16.6 | +0.27 | 68 % |

[†] At $N = 4$ this $R$ is not statistically meaningful (its 95 % CI spans $\approx [-1, 1]$). The aggregate $R = 0.27$ likewise has a wide CI $[-0.21, 0.71]$; at these sample sizes RMW quality is better judged by bias, MAE and hit-rate than by $R$.

Where QiFeng does place a tight-eye case too far out, the cause is that the CYGNSS sampling cannot resolve a tight eyewall. The reconstruction is output on a 1.5 km grid, but it is constrained by CYGNSS specular-point observations, each with a $\sim 25 \times 25$ km footprint and sampled sparsely and irregularly, with no imaging swath. When the true eyewall is tighter than the footprint ($\lesssim$25 km) the observations cannot place the wind maximum that far inward, and the azimuthal-mean peak can be smeared radially outward, as for Emnati and Fiona, which sit well above the 1:1 line in Fig. R2. This footprint limit accounts for the largest positive outliers, but it is not the whole story: for some storms QiFeng instead places the RMW too far *in* (see the TDR comparison below), and the weak-storm scatter has a different origin (broad, ill-defined wind maxima). The low aggregate $R = 0.27$ therefore reflects a combination of this resolution floor, genuine bidirectional errors, and a small, noisy sample spanning a narrow RMW range.

The reference also carries real uncertainty and is itself a substantial part of the scatter. A single SAR overpass is an instantaneous snapshot; eyewall heavy rain and high winds saturate the C-band retrieval, and, as the audit above shows, a large fraction of overpasses cannot yield a QC-passing eye centre. The SAR RMW therefore carries an uncertainty of the same order as the QiFeng error.

The airborne-TDR comparison makes clear that the RMW depends on how it is defined, so we report it both ways. TDR is the tail-Doppler radar on the NOAA P-3 aircraft; TC-RADAR v3 merges the multiple passes of one flight into a single re-centred three-dimensional wind field (Fischer et al., 2022), and 24 OCS-pass times in 2020–2022 match a reconstruction, 22 of which yield a clean field-derived RMW (Fig. R2b). Where the RMW is physically well defined, in storms with a clear eyewall, QiFeng

agrees closely with TC-RADAR's own operational RMW (`tc_rmw`, the radius of the 2 km azimuthal-mean tangential-wind maximum, with its own centre-finding): the bias is +1.5 km for Cat 1–2 and −2.3 km for Cat 3–5. The overall bias against `tc_rmw` is −19.6 km, but this is dominated by the weak TD/TS cases, for which no compact eyewall exists and the operational tangential-wind RMW is itself ill defined (median ≈112 km). Computing the RMW the same way on both sides — as the radius of the azimuthal-mean wind-speed maximum from the same TDR field, exactly as for QiFeng — removes the definitional mismatch and gives a bias of +5.9 km, but with a scatter (MAE 24 km, $R = 0.23$, $N = 22$) that is, if anything, larger than against SAR. Neither TDR estimate is ground truth; both carry their own uncertainty, and we report both. The honest summary across both references is therefore: the *net* RMW bias is small (+5 to +6 km), but the case-to-case error is large and of both signs (MAE ≈17–24 km). The two references do not even agree on the sign for the most intense storms — against SAR the Cat 3–5 bias is +22.5 km, whereas against the TDR field it is slightly negative (≈ −4 km, with individual cases such as Larry and Delta placed too far *in*) — in part because the P-3 aircraft sample only Atlantic/East-Pacific storms, so the small-eye Indian-Ocean cases that dominate the SAR positive bias are absent from the TDR set. We will add Figs. R2–R3 and these statistics, state plainly under "Known limitations" that an individual RMW should be treated as uncertain by roughly ±15–25 km (more in the most intense, small-eye storms), and give concrete guidance for users who need a precise RMW.

It is also worth addressing the specific Fig. 1 and Fig. 2 values you cite, for which Fig. R3 collects the multi-source RMW.

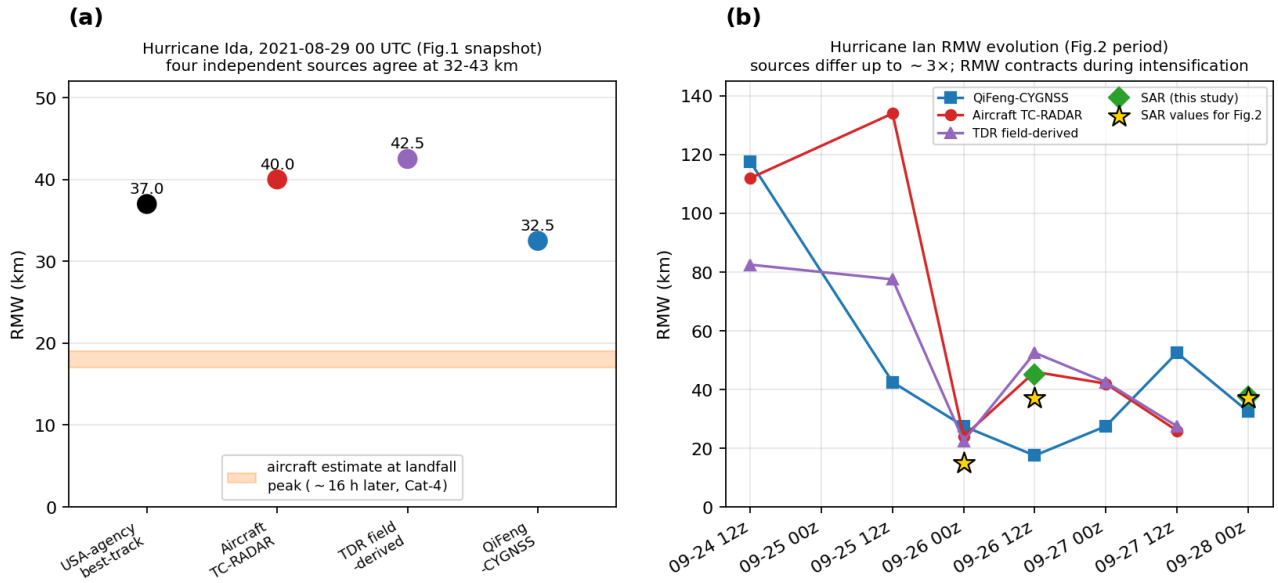


**Fig. R3.** Multi-source RMW for the two cases you raise. (a) Hurricane Ida at the Fig. 1 snapshot time; (b) Hurricane Ian RMW evolution over the Fig. 2 period.

For Fig. 1 (Ida, 2021-08-29 00 UTC; $V_{\max} = 90$ kt, Cat 2), two independent platforms place the RMW in a narrow range at that reporting time — the USA best-track at 37 km and the airborne TC-RADAR at ≈37–43 km (its 2 km tangential-wind `tc_rmw` and its field-derived wind-speed RMW give similar values) — and QiFeng gives 32.5 km, consistent with them and slightly on the inner side. Ida then intensified rapidly with a sharply contracting eyewall, and by its Category-4 landfall about 16 h later the eye had narrowed considerably (NHC reports an eye about 15 n mi wide at landfall; Beven et al., 2022), consistent with the smaller 17–19 km aircraft estimate you cite. The Fig. 1 snapshot and the

landfall time therefore sample different stages of the same intensifying, contracting vortex, which is exactly your point that the RMW varies strongly with time and source.

For Fig. 2 (Ian), the preprint shows the CYGNSS input, the QiFeng reconstruction and CCMP side by side. Ian was rapidly intensifying with a contracting eyewall over this period, so the RMW changes substantially within hours and nearby sources differ by up to a factor of ∼3 (Fig. R3b). Given this strong time dependence we will not treat any single-scene RMW as a fixed "truth" but will instead characterise RMW quality through the aggregate statistics of Fig. R2; in practice we will adjust the Fig. 2 axes and caption so the RMW values are not read in isolation, and cite Fig. R3 when discussing the time and source sensitivity of the RMW.

Your third suggestion was an estimate of the wavenumber-1 (WN1) asymmetry quality as a function of radius, which we give in Fig. R4.

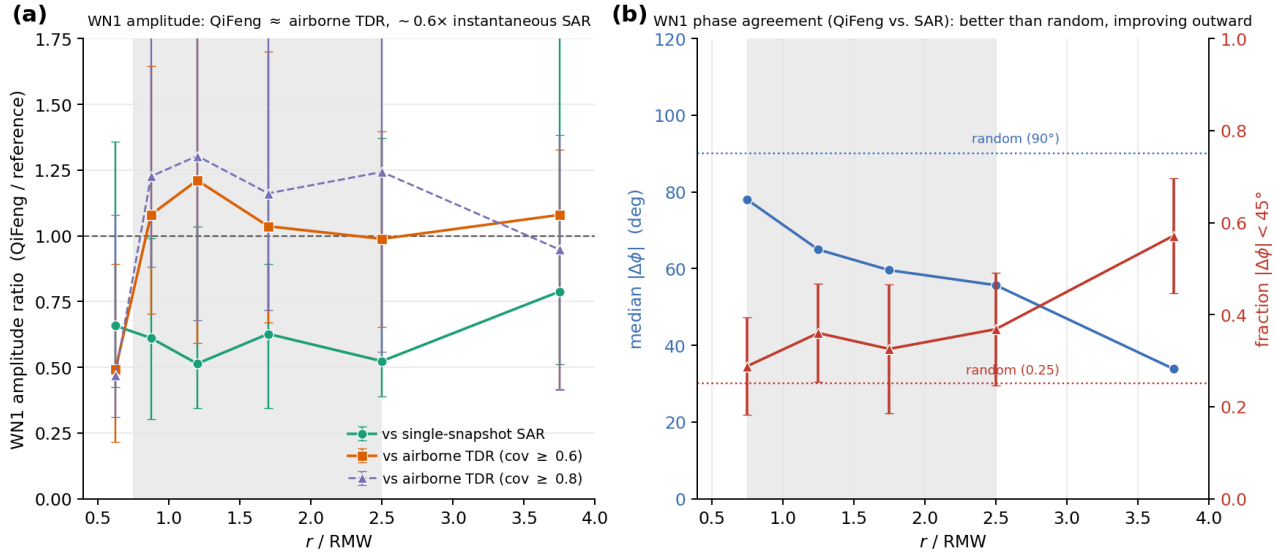


**Fig. R4.** Quality of the WN1 asymmetry, on the same audited OCS-pass sample. (a) WN1 *amplitude* recovered by QiFeng, as the QiFeng/reference amplitude ratio vs. normalised radius, against *two independent* references that bracket the answer: a single-snapshot C-band SAR and the airborne TDR composite (the latter at two azimuthal-coverage thresholds, ≥0.6 and ≥0.8). Estimator: ratio-of-medians with 95 % cluster-bootstrap CIs (resampling whole storms, so correlated radial rings are not counted as independent). (b) WN1 *phase* agreement between QiFeng and the co-located SAR snapshot — the paired phase difference $|\Delta\phi|$ vs. $r$/RMW (median, left axis) and the fraction within 45° (right axis); dotted lines mark the random-chance levels (90°; 0.25).

For amplitude we use a single estimator (ratio-of-medians) with 95 % cluster-bootstrap CIs and bracket the answer between two independent references. In the eyewall band ($0.75 \le r/\mathrm{RMW} < 2.5$) QiFeng recovers about 1.0 of the airborne-TDR amplitude (ratio 1.04, CI $[0.76, 1.42]$ at azimuthal coverage ≥0.6; 1.20, CI $[0.83, 1.69]$ at ≥0.8) and about 0.6 of the instantaneous-SAR amplitude (0.57, CI $[0.40, 0.83]$). The two point estimates differ by a factor of ≈1.8 and their CIs overlap only marginally, and only at the looser ≥0.6 threshold, so we do not claim the two references agree — we use them as a bracket. Tightening the TDR azimuthal-coverage threshold from 0.6 to 0.8 does not lower the TDR ratio (it rises), so the ≈1.0 result against TDR is not an artefact of partial azimuthal sampling of the TDR merge. The two references do agree on where QiFeng is weakest: the innermost core ($r \lesssim 0.75$ RMW, $\lesssim$25 km; ratio ≈0.5), at the CYGNSS footprint scale. The gap between the two references is itself expected: an instantaneous single-pass SAR snapshot carries the highest WN1

amplitude, because transient features, retrieval noise and partial azimuthal coverage all project onto WN1, whereas the multi-pass TDR merge is a smoothed analysis with an effective resolution close to the reconstruction. We therefore report the amplitude as this SAR–TDR bracket rather than a single number: in *magnitude* QiFeng is statistically comparable to the smoothed TDR analysis and about 0.6 of the noisier instantaneous SAR, but the *case-to-case* amplitude correlation is weak (near zero in several radial bands), so a per-storm asymmetry amplitude should not be over-interpreted. We will present the bracketed amplitude (Fig. R4a) and note both the innermost-core low bias and the weak case-to-case correlation under "Known limitations".

The phase is a genuine but modest skill that improves outward. The paired QiFeng-versus-SAR WN1 phase difference (Fig. R4b) has a median $|\Delta\phi|$ that falls from $\approx$78° in the inner core ($r$/RMW $\approx 0.75$) to $\approx$34° in the outer core ($r$/RMW $\approx 3.75$), while the fraction within 45° rises from 0.29 to 0.57 — better than the random baseline (90°; 0.25) in every band. As you suggested, we also examined the phase in a motion-relative framework (per-storm phase concentration about the heading): there both fields are only weakly concentrated — even the SAR reference reaches only $R_{\mathrm{SAR}} \approx 0.40$, with QiFeng at $R_{\mathrm{QiFeng}} \approx 0.21$, against a chance level of $\approx 0.20$. This is physically expected, because inner-core asymmetry is organised primarily by environmental vertical wind shear rather than by storm motion (Uhlhorn et al., 2014; Klotz & Jiang, 2016; Chen et al., 2006), so the motion-relative frame is intrinsically weakly concentrated even for the reference, and an instantaneous single-platform snapshot constrains the absolute phase poorly. We therefore report the phase mainly as agreement with the co-located SAR (Fig. R4b), and recommend caution wherever a precise WN1 phase is required.

In short, in the eyewall and outer core QiFeng reproduces the *magnitude* of the WN1 asymmetry — statistically comparable to the smoothed airborne TDR and about 0.6 of the noisier instantaneous SAR, though with weak case-to-case correlation — and underestimates it only in the innermost $\sim$25 km; it recovers the orientation of the asymmetry with a modest, better-than-random skill that improves outward.

In summary, the product describes the inner-core wind speed well at the pixel level (near-zero aggregate SAR bias; outer-core RMSE $\approx 5\,\mathrm{m\,s^{-1}}$). The absolute RMW carries a large case-to-case uncertainty (MAE $\approx$17–24 km depending on the reference) around a small net bias (+5 to +6 km); the error is largest, and the two references least consistent, for intense small-eye storms whose RMW falls below the $\sim$25 km CYGNSS footprint. The WN1 asymmetry amplitude is comparable in magnitude to the smoothed airborne TDR (and $\approx$0.6 of the noisier SAR) in the eyewall and outer core but is underestimated in the innermost $\sim$25 km, and its case-to-case correlation and absolute phase are only modestly better than chance. These sit alongside the high-wind $V_{\max}$ low bias from GNSS-R saturation. These are genuine limitations of the product: they are fundamentally bounded by the $\sim$25 km CYGNSS specular-point footprint and its sparse, irregular sampling, which cannot resolve a tight eyewall, while reconstruction error and the references' own uncertainty add to the case-to-case scatter. We will document each, with its cause and concrete usage guidance, under "Known limitations".

*I also have a few comments that pertain to the introduction of this being the only option around, and some issues that need to be clarified.*

We take this point, and we will revise the abstract, introduction and conclusions to remove any "only/first" framing and to position QiFeng-CYGNSS as complementary to existing operational and reanalysis products (including the NESDIS analysis below), describing clearly what it adds — kilometre-scale vector inner-core fields with multi-basin coverage — rather than what others lack.

*Missing acknowledgement of like datasets: NESDIS has a km-scale tropical cyclone surface wind analysis that provides 3-hourly estimates of surface vector winds. The original method was documented in this paper.*

*Knaff, J. A., M. DeMaria, D. A. Molenar, C. R. Sampson, and M. G. Seybold, 2011: An automated, objective, multi-satellite platform tropical cyclone surface wind analysis. J. of Applied Meteorology and Climatology. 50(10), 2149-2166. doi: 10.1175/2011JAMC2673.1.*

*And real-time estimate available from this website with the data being available from NOAA CLASS.*

*https://www.ospo.noaa.gov/products/ocean/tropical/mtcswa/*

*https://www.ncei.noaa.gov/access/metadata/landing-page/bin/iso?id=gov.noaa.ncdc:C01683*

Thank you for pointing this out; it is a relevant product we should have cited. We will add a discussion and citation of the NESDIS Multiplatform Tropical Cyclone Surface Wind Analysis (MTCSWA; Knaff et al., 2011), with links to the real-time product (OSPO) and the archive (NOAA CLASS), and add MTCSWA to the product-comparison table. The two are complementary: MTCSWA provides operational, 3-hourly, multi-platform blended vector wind analyses, whereas QiFeng-CYGNSS provides 1.5 km, CYGNSS GNSS-R-based inner-core vector reconstructions.

*Clarification: IBTRaCS is an amalgamation of best track dataset from many agencies including Warning Centers and WMO RSMCs. Could you clarify which best tracks from IBTRaCs are being used. If NHC and JTWC are indeed used as I suspect can you provide the references to those best tracks. NHC's reference is https://doi.org/10.1175/MWR-D-12-00254.1 and JTWC reference (very recent) is https://www.metoc.navy.mil/jtwc/products/best-tracks/JTWC_TC_Best_Tracks_NRL_Report.pdf. Both reports discuss uncertainties associated with intensity and structure. This information probably should be part of your write up.*

As you suspected, we use the USA-agency best tracks in IBTrACS (Knapp et al., 2010): NHC for the North Atlantic and the Eastern/Central Pacific, and JTWC for the Western Pacific and the remaining basins. We will state this explicitly in Data and Methods and add the references (NHC: Landsea & Franklin, 2013; JTWC: Howell et al., 2025), and we will summarise the intensity- and structure-uncertainty discussions in those reports and connect them to the RMW and asymmetry uncertainties quantified above.

## References


Beven, J. L., II, A. Hagen, and R. Berg, 2022: *Hurricane Ida (AL092021).* NOAA/NWS National Hurricane Center Tropical Cyclone Report, 4 April 2022. https://www.nhc.noaa.gov/data/tcr/AL092021_Ida.pdf

Chen, S. S., J. A. Knaff, and F. D. Marks Jr., 2006: Effects of vertical wind shear and storm motion on tropical cyclone rainfall asymmetries deduced from TRMM. *Mon. Wea. Rev.*, 134, 3190–3208. https://doi.org/10.1175/MWR3245.1

Fischer, M. S., R. F. Rogers, P. D. Reasor, and J. F. Gamache, 2022: An analysis of tropical cyclone vortex and convective characteristics in relation to storm intensity using a novel airborne Doppler radar database. *Mon. Wea. Rev.*, 150, 2255–2278. https://doi.org/10.1175/MWR-D-21-0223.1

Howell, B., M. Kucas, L. Cowan, B. Strahl, A. Howard, and C. R. Sampson, 2025: *The Joint Typhoon Warning Center Tropical Cyclone Best Tracks, 1945–2025.* Naval Research Laboratory, Washington, DC, Rep. NRL/7550/FR–2025/3, 29 September 2025. https://www.metoc.navy.mil/jtwc/products/best-tracks/JTWC_TC_Best_Tracks_NRL_Report.pdf (last access: 22 June 2026).

Knaff, J. A., M. DeMaria, D. A. Molenar, C. R. Sampson, and M. G. Seybold, 2011: An automated, objective, multiple-satellite-platform tropical cyclone surface wind analysis. *J. Appl. Meteor. Climatol.*, 50, 2149–2166. https://doi.org/10.1175/2011JAMC2673.1

Knapp, K. R., M. C. Kruk, D. H. Levinson, H. J. Diamond, and C. J. Neumann, 2010: The International Best Track Archive for Climate Stewardship (IBTrACS): Unifying tropical cyclone best track data. *Bull. Amer. Meteor. Soc.*, 91, 363–376. https://doi.org/10.1175/2009BAMS2755.1

Klotz, B. W., and H. Jiang, 2016: Global composites of surface wind speeds in tropical cyclones based on a 12-year scatterometer database. *Geophys. Res. Lett.*, 43, 10 480–10 488. https://doi.org/10.1002/2016GL071066

Landsea, C. W., and J. L. Franklin, 2013: Atlantic hurricane database uncertainty and presentation of a new database format. *Mon. Wea. Rev.*, 141, 3576–3592. https://doi.org/10.1175/MWR-D-12-00254.1

Uhlhorn, E. W., B. W. Klotz, T. Vukicevic, P. D. Reasor, and R. F. Rogers, 2014: Observed hurricane wind speed asymmetries and relationships to motion and environmental shear. *Mon. Wea. Rev.*, 142, 1290–1311. https://doi.org/10.1175/MWR-D-13-00249.1